

Research



Cite this article: Hutchinson JW, Thompson JMT. 2017 Nonlinear buckling behaviour of spherical shells: barriers and symmetry-breaking dimples. *Phil. Trans. R. Soc. A* **375**: 20160154.
<http://dx.doi.org/10.1098/rsta.2016.0154>

Accepted: 1 December 2016

One contribution of 13 to a theme issue
'Patterning through instabilities in complex
media: theory and applications.'

Subject Areas:

mechanical engineering

Keywords:

spherical shells, post-buckling,
non-axisymmetric buckling

Author for correspondence:

John W. Hutchinson
e-mail: jhutchin@fas.harvard.edu

Nonlinear buckling behaviour of spherical shells: barriers and symmetry-breaking dimples

John W. Hutchinson¹ and J. Michael T. Thompson²

¹School of Engineering and Applied Sciences, Harvard University,
Cambridge 02138, MA, USA

²Department of Applied Maths and Theoretical Physics, University
of Cambridge, Cambridge CB3 0WA, UK

JWH, 0000-0001-6435-3612

The nonlinear axisymmetric post-buckling behaviour of perfect, thin, elastic spherical shells subject to external pressure and their asymmetric bifurcations are characterized, providing results for a structure/loading combination with an exceptionally nonlinear buckling response. Immediately after the onset of buckling, the buckling mode localizes into a dimple at the poles. The relations among the pressure, the dimple amplitude and the change in volume of the shell are determined over a large range of pole deflections. These results allow accurate evaluation of criteria such as the Maxwell condition for which the energies in the unbuckled and buckled states are the same and evaluation of the influences of pressure versus volume-controlled loadings. Non-axisymmetric bifurcation from the axisymmetric state, which occurs deep into the post-buckling regime in the form of multi-lobed dimples, is also established and discussed.

This article is part of the themed issue 'Patterning through instabilities in complex media: theory and applications.'

1. Introduction

Spherical shells under external pressure and cylindrical shells under axial compression have extraordinarily nonlinear buckling behaviour. A spherical shell can buckle catastrophically with a sudden drop in pressure even when a fluid inside the shell permits no change in volume during the dynamic jump. Closely related to this catastrophic behaviour is the highly imperfection-sensitive nature of these two structure/loading combinations such that experimentally measured buckling

loads for thin shells can be as low as 20% of the load for a perfect shell. These facts are well known and there is a large experimental and theoretical literature going back almost 75 years addressing the subject, especially for cylindrical shells under axial compression.

Starting with the work of von Kármán & Tsien [1] and Tsien [2], a major effort was made to come to terms with the catastrophic nature and imperfection sensitivity of the buckling of elastic spherical shells by studying the post-buckling behaviour of the perfect shell, with parallel efforts on cylindrical shells under axial compression. Criteria involving load-carrying capacity and/or energy in the post-buckling state were proposed to explain the low buckling loads measured in tests and to serve as a guide for safe design. While the studies clearly exposed the source of the catastrophic buckling behaviour, the approaches based on behaviour of the perfect shells have not yet been particularly successful in yielding quantitative predictions of imperfection sensitivity.

Approaches which directly account for realistic imperfections in shell construction have been more effective in explaining and predicting the low buckling loads observed in tests. Koiter's [3,4] major contribution to elastic stability theory was to relate the buckling behaviour of the imperfect shell to the post-buckling behaviour of the perfect shell. His approach exploits a perturbation expansion of the post-buckling response of the perfect shell about the bifurcation load combined with the incorporation of imperfections in the shell geometry to predict the reduction in the maximum support load of the shell. The limitations of this type of analysis turn out to be especially severe for the spherical shell buckling problem. The primary reason is that the range of validity of the perturbation expansion for the perfect spherical shell is very small. It has recently been emphasized that the bifurcation mode of the perfect spherical shell, which envelops the entire shell, localizes to a dimple-like buckle immediately after bifurcation [5]. Associated with this mode localization is a transition in the post-buckling response such that the perturbation expansion also loses validity almost immediately. Because the perturbation expansion of the perfect shell is the 'backbone' of the imperfection-sensitivity analysis in the Koiter approach, it follows that the imperfection-sensitivity predictions also have an extremely limited range of validity for spherical shells, as has recently been detailed by Lee, Hutchinson and co-workers [5,6].

The main objective of this paper is to present complete and accurate results for perfect spherical shells subject to external pressure buckling relatively deep into the post-buckling range for all ratios of radius to thickness relevant for thin shells. Surprisingly, such results are not available in the range relevant to structural behaviour, severely constraining prior efforts to establish criteria for structural stability based on the behaviour of the perfect shell. Recent work by Knoche & Kierfeld [7,8] has addressed a wide range of advanced post-buckling modes for very thick shells involving axisymmetric deflections of spherical shells that are both symmetric and unsymmetric with respect to the equator, accounting for deflections deep enough to cause shell surface contact. Such modes generally fall outside the range of structural applicability but are of interest in applications in the life sciences where situations involving full collapse of the shells can be important. An axisymmetric response governs the behaviour of the spherical shell until deep into the post-buckling range and the first part of the present paper will focus on this restricted class of deformations. With accurate results in hand for thin spherical shells, we will re-examine some of the buckling criteria based on the behaviour of the perfect shell. The second part of the paper investigates bifurcation from the axisymmetric state, establishing that, indeed, once it is initiated the axisymmetric dimple buckle does not generate non-axisymmetric bifurcations until relatively deep dimples have formed. These findings are discussed within the context of the variety of asymmetric dimple buckle shapes observed experimentally by Berke & Carlson [9].

Perfect, full spherical shells made of a linear isotropic material with Young's modulus E and Poisson's ratio ν are considered with radius R and thickness t . Euler angles define points on the middle surface with ω as the circumferential angle ($0 \leq \omega \leq 2\pi$) and θ as the meridional angle ($-\pi/2 \leq \theta \leq \pi/2$) with $\theta = 0$ at the equator. The small strain-moderate rotation theory of thin shells [10,11] will be employed to describe the shell. This theory employs as dependent variables the displacement components of the shell middle surface, with u_ω and u_θ as the components tangent to the undeformed surface and w normal to this surface. The applicability and accuracy of

this theory for the spherical shell problem will be discussed throughout the paper. For thin shells, a dimple buckle localizes to a shallow region at the pole, and small strain–moderate rotation theory reduces to shallow shell theory in these regions. We will exploit aspects of shallow shell theory in developing a complete characterization of the shell behaviour. The paper draws heavily on the earlier paper by Hutchinson [5], and the reader will be directed to this earlier paper for the governing shell equations and the numerical methods.

2. Axisymmetric buckling behaviour of perfect, thin spherical shells

The results presented in this section characterize the axisymmetric post-bifurcation behaviour of perfect thin elastic spherical shells buckling symmetrically with respect to the equator. The results are ‘universal’ in the sense that they are valid for all radius-to-thickness ratios R/t above about 50 and for any Poisson’s ratio, ν , subject to a constraint on the amplitude of the buckling deflection. The simplicity of the results stems from the shallow nature of the dimple-like buckles at the poles when R/t is sufficiently large, as will emerge clearly from this article. It will also be noted that the results do not correctly reproduce the post-buckling response immediately after bifurcation. The primary interest is to characterize the post-buckling behaviour of the shell in the range of moderate to advanced deflections.

With p as the external pressure, $p_C = 2E(t/R)^2 / \sqrt{3(1-\nu^2)}$ is the classical buckling pressure of the perfect shell with modulus E , and $w_C = (1-\nu)t / \sqrt{3(1-\nu^2)}$ is the uniform inward radial displacement of the unbuckled shell when $p = p_C$. Let w_0 be the uniform inward radial displacement at p in the unbuckled solution which satisfies $w_0/w_C = p/p_C$. Denote the (inward) radial displacement in the axisymmetric buckled state by $w(\theta)$ and its value at the poles by $w_{\text{pole}} = w(\pi/2)$. As discussed in the Introduction, buckling localizes in the form of a dimple at each of the poles (or possibly, as we shall see, to a single dimple at one pole) almost immediately after bifurcation from the uniform state. Away from the poles, the shell asymptotes to the uniform state, $w(\theta) = w_0$, associated with p . In the complete representation of the buckling solution, it is important to separate the uniform deformation state from the non-uniform response. For this purpose, let $\Delta w(\theta) = w(\theta) - w_0$ and $\Delta w_{\text{pole}} = w_{\text{pole}} - w_0$ be the additional inward displacement quantities which are only significantly non-zero in the vicinity of the poles.

As already noted, the primary shell theory used to compute the buckling behaviour of the shell is small strain–moderate rotation theory, but shallow shell theory is also employed to characterize the solution when buckling is localized at the poles. For each theory, the numerical scheme used to generate the results for the axisymmetric response is based on a sixth-order system of nonlinear ordinary differential equations detailed in [5] for the moderate rotation theory. In [5], by drawing comparison with results from a theory employing exact bending and stretching measures for the shell middle surface, it is demonstrated that, for the spherical shell buckling problems of interest in this paper, the moderate rotation theory provides an accurate description of the buckling response for pole deflections as large as $\Delta w_{\text{pole}} = 0.2R$, assuming that the shell is thin enough such that the strains remain small. Solutions to the equations of moderate rotation theory depend on two dimensionless parameters, R/t and ν , and these parameters must be specified to generate any solution. However, moderate rotation theory reduces to shallow shell theory near the poles. Thus, when the buckling deflections are localized at the poles, shallow shell theory pertains. The significance of this for present purposes is that the equations of shallow shell theory for spherical shell buckling can be cast in a dimensionless form which is *independent* of R/t and ν with the dependence on these parameters absorbed into the solution variables. This feature will allow us to present complete results for all R/t and ν . The range of applicability of the results is limited to sufficiently large R/t , as will be made clear. The equations of shallow shell theory make use of the fact that the slopes of the shell are shallow relative to a base plane lying below the region near the pole where the buckling deflections occur. These equations are not listed here but they can be found in [10,11] and the dimensionless form referred to above for spherical shells appears in [12,13].

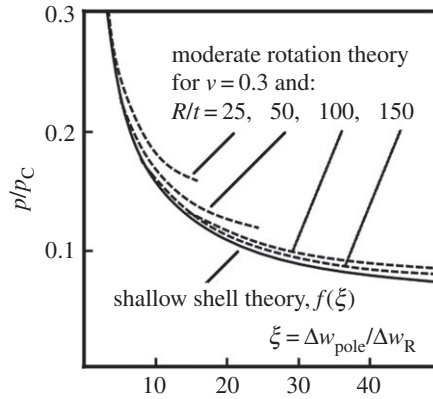


Figure 1. Relation between the pressure and pole buckling deflection for axisymmetric buckling of a perfect spherical shell. The dimple buckle is localized at the poles. The limit of moderate rotation theory as R/t becomes large is $f(\xi)$, and the results of moderate rotation theory are well approximated by $f(\xi)$ if $\xi < 0.2R/t$.

Based on the variables that emerge from rendering the shallow shell equations dimensionless, we introduce the reference deflection Δw_R and the dimensionless pole buckling deflection ξ , where

$$\Delta w_R = \frac{t}{\sqrt{(1-\nu^2)}} \quad \text{and} \quad \xi = \frac{\Delta w_{\text{pole}}}{\Delta w_R}. \quad (2.1)$$

Further, we denote the meridional distance from the upper pole by $s = R(\pi/2 - \theta)$ and define a dimensionless distance from the pole as

$$\tilde{s} = \frac{(1-\nu^2)^{1/4} s}{\sqrt{Rt}}. \quad (2.2)$$

A plot of the normalized pressure as a function of the dimensionless pole buckling deflection is presented in figure 1. The dashed curves in this figure have been computed using moderate rotation theory for several values of R/t with $\nu = 0.3$. The solid curve has been computed using shallow shell theory and it has the form

$$\frac{p}{p_C} = f(\xi), \quad (2.3)$$

with $f(\xi)$ given in table 1 for $\xi \leq 60$. The dependence on R , t and ν in (2.3) is entirely embedded in p_C and Δw_R .

As noted earlier, the goal in this paper is to characterize the buckling response of the shell for relatively large buckling deflections, e.g. $1 < \xi < 60$. The initial post-buckling range immediately following bifurcation is not addressed nor does $f(\xi)$ capture the details of the initial post-bifurcation response before the localization is fully developed. The initial post-bifurcation behaviour for the full sphere was determined by Thompson [14] and Koiter [4]. However, the abrupt transition from the initial post-bifurcation response to localized dimple buckling behaviour alluded to earlier occurs almost immediately after bifurcation. Numerical results in [5] for $R/t \cong 100$ have shown that this transition takes place when $p/p_C > 0.8$ and $\xi < 0.5$. In summary, $f(\xi)$ does not accurately capture the shell behaviour in the range $0 < \xi < 0.5$ but is accurate in the range of larger ξ as long as the dimple is shallow.

Figure 1 reveals that shallow shell theory provides an accurate approximation for p/p_C from moderate rotation theory in a range of $\xi = \Delta w_{\text{pole}}/\Delta w_R$ that depends on R/t , which is given approximately by $\xi < 0.2R/t$. The larger the R/t , the wider the range of ξ for which $p/p_C = f(\xi)$ is accurate. The limit of the moderate rotation theory for any fixed ξ as R/t becomes large is the shallow shell result $f(\xi)$. Although not plotted, the moderate rotation theory results for $R/t = 300$ agree with $f(\xi)$ to within a fraction of 1% for $\xi \leq 60$, and results computed with

Table 1. Function values characterizing dimple buckling of a perfect spherical shell determined using shallow shell theory with ξ as the normalized pole deflection defined in (2.1). Cubic splines provide an accurate interpolation of the values listed.

ξ	$f(\xi)$	$h(\xi)$	$q(\xi)$
0	1.0000	0.0000	0.0000
1	0.6280	0.1867	0.1405
2	0.4130	0.6782	0.3840
3	0.3127	1.515	0.6795
4	0.2592	2.747	1.027
5	0.2260	4.417	1.429
6	0.2031	6.557	1.886
7	0.1858	9.186	2.395
8	0.1722	12.32	2.956
9	0.1612	15.97	3.563
10	0.1517	20.14	4.214
15	0.1209	48.92	8.058
20	0.1034	90.70	12.70
25	0.0918	145.0	17.97
30	0.0834	211.8	23.80
35	0.0770	290.8	30.12
40	0.0719	382.3	36.92
45	0.0677	486.4	44.17
50	0.0641	603.0	51.84
55	0.0611	731.9	59.91
60	0.0584	873.2	68.34

$R/t = 500$ reproduce the values for $f(\xi)$ listed in table 1. Additionally, it is shown in [5] that the assumptions regarding rotations underpinning the accuracy of moderate rotation theory are met for the axisymmetric spherical shell buckling problem if $w_{\text{pole}}/R < 0.2$, which is essentially the same as the requirement on the equivalence of the shallow and moderate rotation shell theories, i.e. $\xi < 0.2R/t$. In summary, (2.3) provides an accurate result for the post-buckling response of the shell if $0.5 < \xi < 0.2R/t$.

For buckling deflections localized near the pole, the solution to shallow shell theory for the additional normal displacement has the form

$$\frac{\Delta w}{\Delta w_R} = g(\tilde{s}, \xi) \quad (2.4)$$

with no further dependence on R/t and ν . The dimple shape $g(\tilde{s}, \xi)$ is plotted in figure 2.

The meridional extent of the dimple for $\xi = 50$ measured from the pole to its edge is approximately $\tilde{s}_{\text{edge}} = 10$. By (2.2), this implies that the angle from the pole to the dimple edge is

$$\beta \cong \frac{10}{(1 - \nu^2)^{1/4}} \sqrt{\frac{t}{R}} \quad \text{at } \xi = \frac{\Delta w_{\text{pole}}}{\Delta w_R} = 50. \quad (2.5)$$

The larger the R/t , the smaller the polar angle of the dimple buckle. For $R/t = 300$, a dimple having a pole deflection $\xi = 50$ has $\beta \cong 0.6$ ($\cong 35^\circ$). Separate calculations using moderate rotation

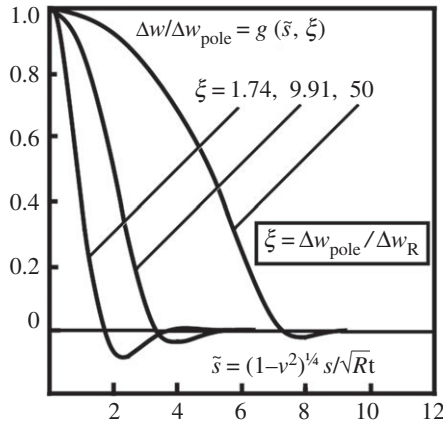


Figure 2. Shape of the dimple buckle as predicted by shallow shell theory.

theory verify that the predicted dimple shape is in very close agreement with the shallow shell results as long as β is not greater than about 35° .

The decrease in volume contained within the shell middle surface is $\Delta V = \int_S w \, dS$, with S as the shell middle surface. The decomposition, $\Delta w(\theta) = w(\theta) - w_0$, implies

$$\Delta V = \int_S w_0 \, dS + \int_S \Delta w \, dS. \quad (2.6)$$

This is the linearized expression for the volume change, but it has been shown in [5] that the difference between the exact volume change and that from (2.6) is a small fraction of a per cent for the sphere buckling problem if $w_{\text{pole}}/R < 0.2$. If the dimple is shallow, then Δw from (2.4) in (2.6) yields the dimensionless relation

$$\frac{\Delta V}{\Delta V_C} = f(\xi) + C \frac{t}{R} h(\xi) \quad \text{with } h(\xi) = \xi \int_0^{\xi_{\text{edge}}} g(\xi, \xi) \xi \, d\xi, \quad (2.7)$$

where

$$\left. \begin{aligned} C &= \frac{\sqrt{3}}{(1-\nu)\sqrt{1-\nu^2}} \\ \Delta V_C &= 4\pi R^2 w_C = \frac{4\pi(1-\nu)R^2 t}{\sqrt{3}(1-\nu^2)}. \end{aligned} \right\} \quad (2.8)$$

The decrease in volume of the shell (2.7) based on the shallow shell theory characterization of the dimple contains all the dependence on R/t and ν . It assumes that the buckling deflection is symmetric with respect to the equator such that there are identical dimples at the top and bottom poles. If there is only one dimple, say at the top pole, then (2.7) is still valid if one replaces C by $C/2$. The function $h(\xi)$ is plotted in figure 3 with values listed in table 1.

We will also have use for the elastic strain energy, U , in the shell in the buckled state. This can be computed directly as the work done by the pressure through the change in volume. Using $p/p_C = \Delta V/\Delta V_C$ prior to buckling and (2.7) for shallow buckles, one obtains for $\xi > 0$

$$\frac{U}{p_C \Delta V_C} = \frac{1}{2} f(\xi)^2 + C \frac{t}{R} q(\xi) \quad \text{with } q(\xi) = \int_0^\xi f(\xi) \frac{dh(\xi)}{d\xi} d\xi \quad (2.9)$$

with $q(\xi)$ plotted in figure 3 and listed in table 1. If there is only one dimple, C must again be replaced by $C/2$.

Calculations have been carried out using moderate rotation theory for a wide range of R/t and various ν that have verified that (2.7) and (2.9) are accurate if the same restrictions on shallowness and moderate rotations are met as those discussed for the relation $p/p_C = f(\xi)$

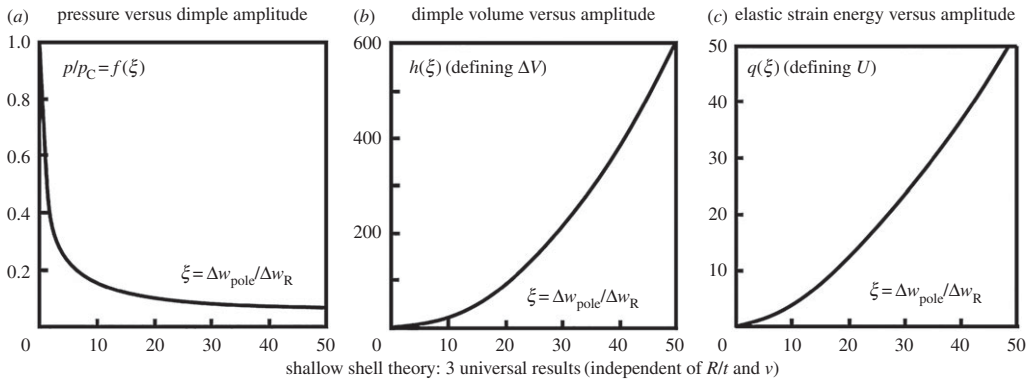


Figure 3. (a–c) Functions defining the shallow dimple buckling for a perfect spherical shell. The functions are computed using shallow shell theory with $f(\xi) = p/p_c$ in (2.3), $h(\xi)$ appearing in ΔV in (2.7) and $q(\xi)$ appearing in U in (2.9).

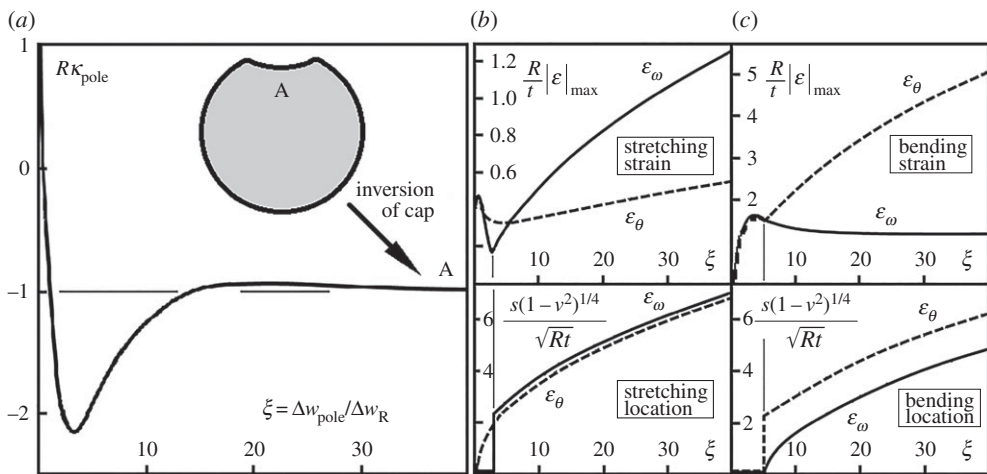


Figure 4. (a) The normalized curvature at the pole. (b) The maximum magnitude and location of the strains in the shell due to stretching at the middle surface and (c) those at the surface due to bending. These normalized plots are computed using shallow shell theory and are independent of R/t . The curves for the curvature at the pole and the strains due to bending are independent of ν , while the curves for the strains due to stretching depend on ν and have been computed with $\nu = 0.3$.

in (2.3). In particular, the constraint

$$\xi \equiv \frac{\Delta w_{\text{pole}}}{\Delta w_R} < 0.2 \frac{R}{t} \quad (2.10)$$

serves as a combined condition ensuring shallow dimple buckles and the applicability of moderate rotation theory. This condition is approximately equivalent to $\Delta w_{\text{pole}} < 0.2R$. It is worth repeating that the relations expressed by (2.3), (2.7) and (2.9) contain the exact dependence on ν and R/t from shallow shell theory and the functions f , h and q listed in table 1 have been computed numerically to an accuracy of three significant places.

With ε_ω and ε_θ as the circumferential and meridional middle surface strains, the uniform strains at the critical buckling pressure are $\varepsilon_\omega = \varepsilon_\theta = -[(1-\nu)/\sqrt{3(1-\nu^2)}](t/R)$. For buckling deflections satisfying (2.10), shallow shell theory provides accurate predictions for the shell curvature and the stretching and bending strains in the shell. Selected results are plotted in figure 4. These plots are independent of R/t . The curvature at the pole becomes slightly more negative than $-2/R$ before attaining the curvature of an inverted cap, $-1/R$, at $\xi > 10$. The normalized strains plotted are the maximum values of the strain magnitudes due to stretching

and bending (at the shell surface). The distance from the pole at which the maximum is attained is plotted below the strain. Thus, for example, for $\xi < 5$ the maximum of each bending strain component occurs at the pole. The location of the maximum of the bending component $|\varepsilon_\omega|$ shifts continuously away from the pole for $\xi > 5$ with $|\varepsilon_\omega|$ varying smoothly, while the location of the maximum of $|\varepsilon_\theta|$ jumps discontinuously from the pole to the region of high negative curvature away from the pole (see figure 2), giving rise to the discontinuity of slope in the variation of the maximum of $|\varepsilon_\theta|$. These plots are useful in determining whether shell buckling behaviour can be modelled by a linear stress–strain relation (as has been done in this paper) or whether nonlinear stress–strain behaviour intervenes. In this regard, it is noted that most metals undergo nonlinear plastic deformation at strains well below 10^{-2} , placing clear limits on the minimum value of R/t for the shell to buckle elastically.

We conclude this section by noting that Evkin *et al.* [12] have employed shallow shell theory together with an asymptotic analysis of the dimple buckle to derive a representation of the dimple deflection (2.4) and expressions for the relation of the pressure to the pole deflection and the energy associated with the dimple, all of which embed the dependence on R/t and ν in a similar manner to the results in this paper. Their asymptotic analysis invokes the inverted cap near the pole, having curvature $-1/R$, which was remarked on earlier with an internal boundary layer governing the transition to the outer uniform solution. Earlier work by Holst & Calladine [13] developed the asymptotic form of the solution for this and other dimple-like shell buckle problems. In the present notation, the asymptotic result for relation (2.3) from [12] is $p/p_C = 0.449/\sqrt{\xi}$, and the elastic strain energy associated with two dimples (at the upper and lower poles) is $U_{\text{dimple}}/p_C \Delta V_C = 0.150(Ct/R)\xi^{3/2}$. The simple formula for p/p_C is in error by about 25% for $\xi \leq 2$, by 7% for $\xi = 10$, and becomes an increasingly accurate approximation to $f(\xi)$ in table 1 as ξ becomes even larger. The error for $\xi < 10$ is not surprising given that the inverted cap representation at the pole is only attained for $\xi > 10$, as seen in figure 4. The formula for the dimple energy is more accurate: at $\xi = 1$, $0.150\xi^{3/2}$ only exceeds $q(\xi)$ in table 1 by 7%, and for $\xi = 50$ it is within 2%. Using $U_{\text{dimple}} = \int p \, d\Delta V$, we have extracted the corresponding asymptotic formula for the volume change associated with the dimple from the other two results, obtaining for the case of two dimples: $\Delta V_{\text{dimple}}/\Delta V_C = 0.251(Ct/R)\xi^2$. The accuracy of $0.251\xi^2$ compared with $h(\xi)$ is similar to that for the pressure–pole relation. In summary, the present results and those of Evkin *et al.* [12] have precisely the same dependence on R/t and ν , and the simple asymptotic formulae for $f(\xi)$, $h(\xi)$ and $q(\xi)$ obtained in [12] and listed above are accurate for large ξ . It should be mentioned that the asymptotic formulae are not meant to be applied for small ξ . Indeed, Evkin *et al.* carry out a modified analysis in an attempt to more accurately capture the behaviour in the transition to the large deflection regime in which the inverted cap solution applies.

3. Pressure–volume relation and equal-energy conditions for full spherical shells

To illustrate the applicability of the relations in §2, we have plotted the pressure as a function of the change in volume in figure 5 for several values of R/t for $\nu = 0.3$ using (2.3) and (2.7). Unlike the relation of pressure to pole buckling amplitude in (2.3), the pressure–volume change relation depends on R/t , as is evident from (2.7). The larger the R/t , the more dramatic the drop in the pressure in the buckling response. At the expense of being overly repetitive, we note that the results in figure 5 have also been computed directly using moderate rotation theory giving a plot that is indistinguishable from that shown. Quilliet [15] has computed curves of pressure versus volume change for spherical shells characterized by an elastic strain energy density that is different from the standard shell theory energy density employed in this study and in [5]. The energy density in [15] is representative of energy functions used to model bilayers in biological cell walls. Nevertheless, the general features of the relations of pressure versus volume change are qualitatively similar, although the numerical method in [15] does not generate the equilibrium curve of the buckled states in the range $\Delta V/V_C < 1$.

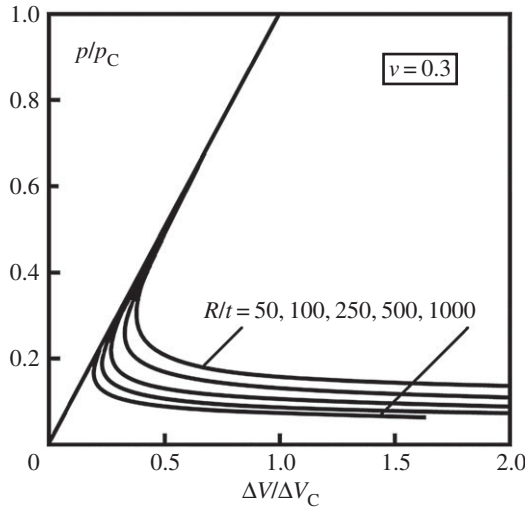


Figure 5. Normalized relation between the pressure and the change in volume for full spherical shells undergoing axisymmetric buckling that is symmetric with respect to the equator.

As a second illustration of the utility of the relations in §2, we determine for rigid volume control the condition, often referred to as Maxwell's condition, wherein the energy in the system in the lower of the two equilibrium buckled states equals the energy in the unbuckled state at the same prescribed ΔV (we discuss the relevance of this later). Because the potential energy of the pressure is the same in these two states, the condition is equivalent to the requirement that elastic energies in shells in the two states are equal. The elastic energy in the unbuckled state is proportional to ΔV^2 while the elastic energy in the buckled state is U in (2.9). In dimensionless form, the equal-energy condition becomes

$$\frac{1}{2} \left(\frac{\Delta V}{\Delta V_C} \right)^2 = \frac{1}{2} f(\xi)^2 + C \frac{t}{R} q(\xi), \quad (3.1)$$

where ξ on the r.h.s. of (3.1) is given in terms of $\Delta V/\Delta V_C$ by (2.7). Making use of (2.7), one finds that the condition (3.1) reduces to the following relation between ξ and Ct/R :

$$C \frac{t}{R} = \frac{2[q(\xi) - f(\xi)h(\xi)]}{h(\xi)^2} = - \frac{2 \int_0^\xi f'(\xi)h(\xi)d\xi}{h(\xi)^2}. \quad (3.2)$$

The associated Maxwell values, p_M/p_C and $\Delta V_M/\Delta V_C$, are then given by (2.3) and (2.7). These values are plotted as a function of the 'universal variable' $(R/t)/C$ in figure 6a and in terms of R/t for $\nu = 0.3$ in figure 6b. Note that the pressure p_O in the unbuckled state is given in these plots as $p_O/p_C = \Delta V/\Delta V_C$. Included in figure 6a is the lowest value of the volume change, $\Delta V_L/\Delta V_C$, for which a buckling solution exists, which is readily obtained as the minimum of $\Delta V/\Delta V_C$ in (2.7) with respect to ξ .

We have seen that the complete spherical shell exhibits a post-buckling path of constantly decreasing external pressure, p , so under (dead) pressure control there is no 'lower buckling load' at which p reaches a minimum within the range of structural interest. This effectively undermines the suggestion by von Kármán & Tsien [1] that this lower load might be used as a practical estimate of the strength of an imperfect shell. Correspondingly, there is no dead load Maxwell condition corresponding to the 'energy criterion' of Tsien [2] at which the trivial uniformly compressed state has the same total energy as a grossly deformed (stable) post-buckling solution. This criterion, based loosely on Maxwell's thermodynamic concept for phase transitions that at a molecular scale a system can be expected to be in its lower energy state, is clearly not valid

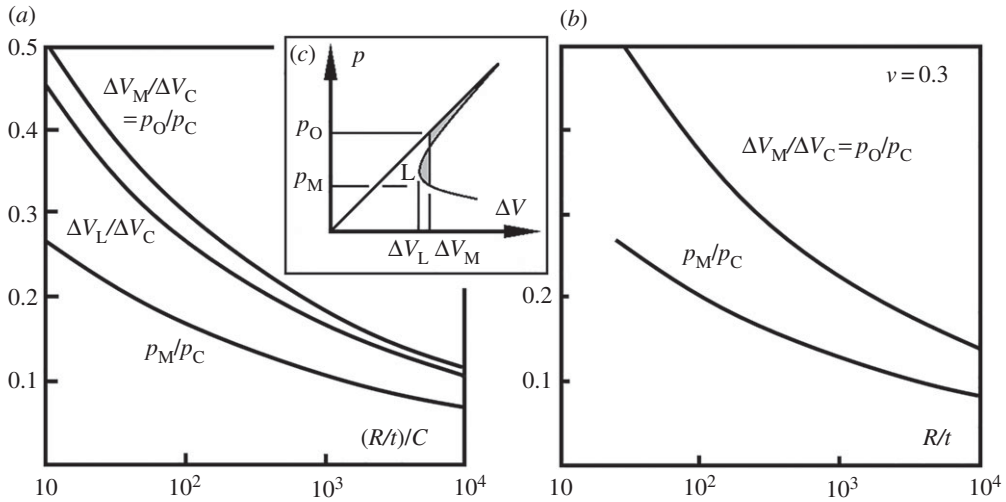


Figure 6. Values of the normalized pressure in the buckled and unbuckled states for a prescribed volume change, $\Delta V/\Delta V_C$, subject to the condition that the energies in the two states are the same. (a) The plot uses the combined parameter, $(R/t)/C$, and (b) the dependence on R/t for $\nu = 0.3$. Panel (a) also includes the lowest value of the volume change, $\Delta V_L/\Delta V_C$, for which a buckling solution exists.

for a shell: since it would, for example, imply that close to the Maxwell load the shell would be continuously jumping into, and back out of, its buckled state. Tsien [16] revoked it himself, and it was also formally disproved by many workers who showed that the failure loads of spheres and cylinders were not dependent on whether they were tested in dead or rigid loading devices as they would be under the energy criterion.

While there is no Maxwell load for the sphere under dead load, the situation is different under the rigid control of the external volume (as we have just evaluated), which is usually the preferred mode of laboratory testing. Here there is a lower buckling condition, at which the post-buckling solution exhibits a minimum of the volume change at point L in figure 6c. These minima, dependent on R/t , are clearly seen in the pressure–volume plots of figure 5. Correspondingly, there is under volume control a Maxwell volume, as displayed in figure 6c, where the two grey areas are equal. We have explored this briefly as above because Maxwell loads have recently been shown to have some real significance (other than the discredited idea of Tsien) in the post-buckling of cylindrical shells under axial compression [17,18]. Thus for the pressure-controlled cylindrical shell the Maxwell load marks the significant appearance of a localized post-buckling deformation, which gives a sudden onset of ‘shock sensitivity’ [19]. This does not carry over in a simple way even to the cylinder under displacement control. So its relevance to our spherical buckling problem is tenuous, especially since the sphere does not feature an independent localized path. Nevertheless, the Maxwell condition is a natural first step in examining the nearby energy barriers against collapse under dynamic disturbances that we examine next in figure 7. It is also worth noting that the dependence of the lower and Maxwell loads on R/t go some way in mirroring the trend of the experimental buckling loads under rigid testing conditions. We shall also be examining semi-rigid loading conditions incorporating the elasticity of the loading system (figure 8).

While discussing cylindrical shells, we should also note the rather unique contribution of Horák *et al.* [20], who used a mathematical searching routine to find the saddle point that gives the lowest energy barrier for an axially compressed cylinder. This saddle point corresponds to a dimple that is localized both axially and circumferentially, suggesting that it could be located experimentally by a rigidly controlled probe [21].

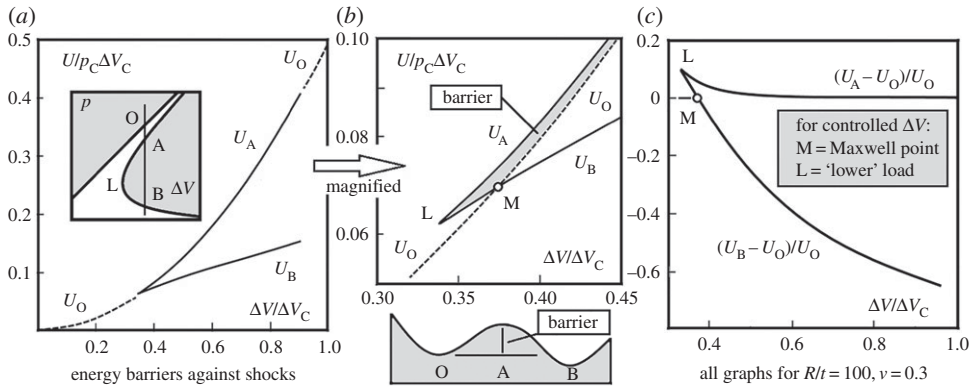


Figure 7. The elastic energy in the shell, U , in the three axisymmetric equilibrium states as a function of the prescribed volume change ΔV where O is the unbuckled state, A is the upper (unstable) equilibrium buckled state and B is the lower buckled equilibrium state. The energy barrier is indicated, as are the Maxwell point and the lowest point L for which buckled states exist. For this figure, $R/t = 100$ and $\nu = 0.3$.

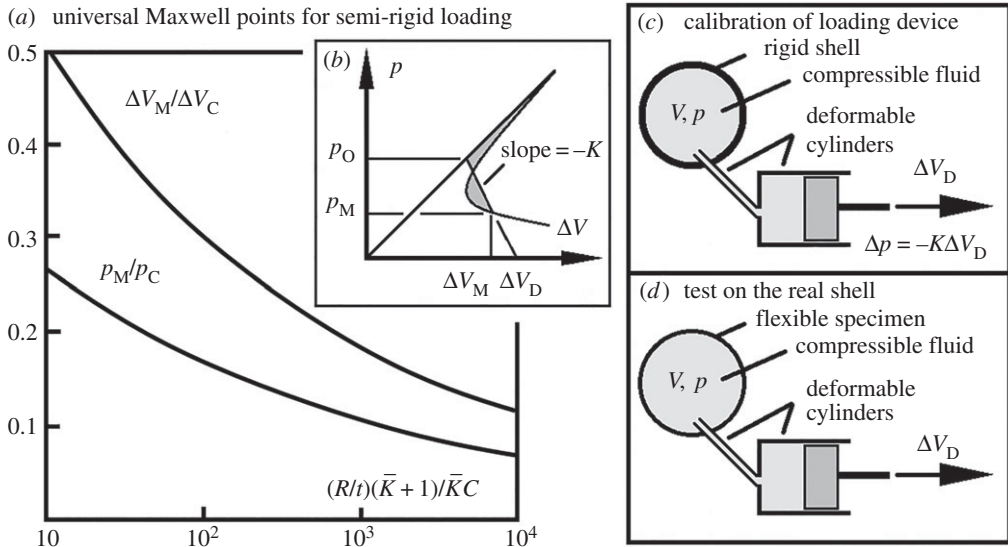


Figure 8. (a–d) Role of system loading compliance in determining the Maxwell point corresponding to equal energies in the system for the unbuckled and buckled shell subject to prescribed ΔV_D .

Further insight into the energy landscape of spherical shell buckling can be gained from figure 7, where the elastic energy U is shown for each of the three equilibrium buckled states, O, A and B, corresponding to the same $\Delta V/\Delta V_C$. State O is the unbuckled state, A is the upper unstable equilibrium state and B is the lower stable equilibrium state. The energies are plotted as a function of $\Delta V/\Delta V_C$ for $R/t = 100$ and $\nu = 0.3$ both in magnitude and in ratio to the energy in the unbuckled shell U_O . The energy associated with A is always greater than that of the unbuckled shell U_O and, as noted in figure 7, this serves as an energy barrier that must be overcome if state B is to be attained. The Maxwell point where $U_B = U_O$ is indicated. As ΔV is increased above the Maxwell point, the relative magnitude of the energy barrier, $(U_A - U_O)/U_O$, decreases while the magnitude of the energy drop from the unbuckled state to the lower buckled state, $U_O - U_B$, significantly increases both absolutely and relatively. The catastrophic nature of spherical shell buckling at loads well above the Maxwell point is driven by this wide energy gap.

We digress briefly to note that a ‘lower buckling load’ under prescribed pressure does exist if the shell is imagined to deform to the extent that the two poles make contact, thereby abruptly stiffening the structure and raising its pressure-carrying capacity. Buckling under a Maxwell constraint of equal energies has been addressed by Knoche & Kierfeld [7,8] under both prescribed volume change and prescribed pressure for their advanced modes involving much larger deflections relative to R than those considered here. These authors have discussed energy barriers for the two loading cases with plots similar to figure 7. The shells for which numerical simulations have been carried out in [7,8] are limited to very thick shells compared with those considered here, i.e. to $R/t < 11$.

The general results in §2 allow the above analysis for the rigid loading of the spherical shell to be extended to a loading system with compliance, e.g. the semi-rigid loading system depicted in figure 8*d*. To calibrate the loading system, replace the actual shell by a rigid shell with the same volume and determine the stiffness K of the system as defined by $p = K\Delta V_D$ with p as the net pressure change in the system (positive acting inward on the shell) and ΔV_D as the prescribed volume change. This relation is assumed to be linear, but the analysis can be extended to include a nonlinear relation at the expense of a more complicated outcome. Note that the system stiffness can derive from both the elasticity of the loading system and the compressibility of the fluid.

As before, denote the volume decrease of the actual shell by ΔV and its value at bifurcation by ΔV_C . For the unbuckled shell in figure 8*d*, one has

$$\frac{p}{p_C} = \frac{\Delta V}{\Delta V_C} = \frac{\bar{K}}{\bar{K} + 1} \frac{\Delta V_D}{\Delta V_C} \quad \text{with} \quad \bar{K} = \frac{K\Delta V_C}{p_C} = \frac{2\pi(1-\nu)KR^4}{Et}. \quad (3.3)$$

The energy in the system at prescribed ΔV_D when the shell is unbuckled is $p\Delta V_D/2$:

$$\frac{E_{\text{unbuckled}}}{p_C\Delta V_C} = \frac{1}{2} \frac{\bar{K}}{\bar{K} + 1} \left(\frac{\Delta V_D}{\Delta V_C} \right)^2. \quad (3.4)$$

In the buckled state, the pressure is related to the volume changes by $p = K(\Delta V_D - \Delta V)$, which with the aid of §2 yields the relation between the pole buckling deflection ξ and ΔV_D :

$$\frac{\bar{K} + 1}{\bar{K}} f(\xi) + C \frac{t}{R} h(\xi) = \frac{\Delta V_D}{\Delta V_C}. \quad (3.5)$$

The energy in the system when the shell is buckled is $\int_0^{\Delta V_D} p dV_D$, including the contributions prior to and after buckling. This energy is

$$\frac{E_{\text{buckled}}}{p_C\Delta V_C} = \frac{1}{2} \frac{\bar{K} + 1}{\bar{K}} f(\xi)^2 + C \frac{t}{R} q(\xi). \quad (3.6)$$

Equating E_{buckled} and $E_{\text{unbuckled}}$, and then making use of (3.5), gives the Maxwell point expressed in terms of ξ

$$\frac{\bar{K}C}{\bar{K} + 1} \frac{t}{R} = \frac{2[q(\xi) - f(\xi)h(\xi)]}{h(\xi)^2}. \quad (3.7)$$

This equation for ξ is precisely equation (3.2) for the rigid loading system with $\bar{K}C/(\bar{K} + 1)$ replacing C .

Because the pressure in the buckled state is $p/p_C = f(\xi)$ and the volume change of the shell is (2.7), independent of the stiffness of the loading system, it follows that the Maxwell plot of p_M and ΔV_M for the rigid loading system in figure 6 converts directly to the semi-rigid system in figure 8*a* if C is replaced by $\bar{K}C/(\bar{K} + 1)$. Decreasing the stiffness of the loading system lowers p_M and ΔV_M . The value of the prescribed volume change ΔV_D at the Maxwell point is given by (3.5), which can also be expressed as

$$\frac{(\Delta V_D)_M}{\Delta V_C} = \frac{\Delta V_M}{\Delta V_C} + \frac{1}{\bar{K}} \frac{p_M}{p_C}. \quad (3.8)$$

The pressure p_O in the unbuckled state associated with $(\Delta V_D)_M$ is given by (3.3). Further discussion of the Maxwell point and the lowest solution limit will be given in the Conclusion.

4. Non-axisymmetric bifurcation from the axisymmetric buckled state

We now address the question of whether the axisymmetric buckling solution characterized in §2 is the only solution or whether non-axisymmetric buckling is likely to occur in the range of interest explored here. To do so, an analysis of non-axisymmetric bifurcation from the axisymmetric buckled state has been carried out. This effort follows earlier work [5] which found no evidence of such bifurcations for moderately large axisymmetric deflections having $\xi = \Delta w_{\text{pole}} / \Delta w_{\text{R}} < 10$. There is experimental evidence [9] discussed later in this section that indicates that non-axisymmetric buckling occurs deep into the post-buckled range, and the investigation here will probe this range. In addition, earlier numerical work searching for energy minima with non-axisymmetric deflections by Quilliet [15] for spherical shells having a different form of strain energy density than that considered here has revealed the existence of such buckling modes.

The axial symmetry of the solutions presented in §2, with dependence only on the meridional angle θ , admits the possibility of non-axisymmetric bifurcation modes in the separated form

$$(u_{\omega}, u_{\theta}, w) = (\bar{u}_{\omega}(\theta) \sin m\omega, \bar{u}_{\theta}(\theta) \cos m\omega, \bar{w}(\theta) \cos m\omega), \quad (4.1)$$

where here the displacements $(u_{\omega}, u_{\theta}, w)$ are additional to the axisymmetric solution, ω is the circumferential angle and $m \geq 1$ is the integer number of circumferential waves in the mode. The functional governing bifurcation can be reduced to a quadratic functional of $(\bar{u}_{\omega}, \bar{u}_{\theta}, \bar{w})$,

$$P_2 \left(\bar{u}_{\omega}, \bar{u}_{\theta}, \bar{w}, m, \frac{\Delta w_{\text{pole}}}{\Delta w_{\text{R}}} \right), \quad (4.2)$$

where $\Delta w_{\text{pole}} / \Delta w_{\text{R}}$ characterizes the amplitude of the axisymmetric solution and is regarded as the eigenvalue of the bifurcation problem. The calculations performed here use moderate rotation shell theory to obtain the axisymmetric solution and to define P_2 . For any m , $P_2 > 0$ for all non-zero admissible functions $(\bar{u}_{\omega}, \bar{u}_{\theta}, \bar{w})$ if $\Delta w_{\text{pole}} / \Delta w_{\text{R}}$ is below the lowest eigenvalue for that m , and P_2 vanishes at the lowest eigenvalue when evaluated in terms of the eigenmode.

The numerical method used to generate the lowest eigenvalue for each m is given in [5]. In brief, cubic splines are used to provide geometrically admissible representations of each of the functions $(\bar{u}_{\omega}, \bar{u}_{\theta}, \bar{w})$ with the set of nodal displacements, a_i , $i = 1 \dots N$, as unknowns. For any given m and each value of $\Delta w_{\text{pole}} / \Delta w_{\text{R}}$, numerical integration is used to evaluate the symmetric $N \times N$ matrix \mathbf{A} defined by

$$P_2 = \sum_{i=1}^N \sum_{j=1}^N A_{ij} a_i a_j. \quad (4.3)$$

The condition for computing the lowest eigenvalue for a given m is the first zero crossing of the determinant of \mathbf{A} as $\Delta w_{\text{pole}} / \Delta w_{\text{R}}$ is monotonically increased. The geometric admissibility of the cubic spline representation ensures that the computed value is an upper bound to the lowest eigenvalue for each m . The non-zero solution to $\sum_{j=1}^N A_{ij} a_j = 0$ when the determinant vanishes provides the bifurcation mode.

The computed eigenvalue for each m , expressed as the value of $\Delta w_{\text{pole}} / \Delta w_{\text{R}}$, is presented in table 2 together with the associated value of p/p_{C} . The values have been computed for a shell with $R/t = 300$ and $\nu = 0.3$. No bifurcation for $m = 1, 2$ or 3 was found in the range $\Delta w_{\text{pole}} / \Delta w_{\text{R}} < 40$. We believe the results in table 2 apply, to a good approximation, for all sufficiently thin spherical shells for reasons which follow. As described in §2, the axisymmetric dimple buckle is localized at the pole with meridional radius no greater than $\bar{s}_{\text{edge}} \cong 10$ if $\Delta w_{\text{pole}} / \Delta w_{\text{R}} < 50$ (see (2.2) and figure 2). Similarly, the non-axisymmetric bifurcation mode is localized at the pole with comparable meridional extent. Thus, for thin shells, the non-axisymmetric buckle is confined to a shallow section of the shell and is governed by shallow shell theory. As was the case for the axisymmetric buckle, the dimensionless form used to present the results for the eigenvalue problem derives from shallow shell theory and contains all the dependence on R/t and ν .

The dimensionless resultant membrane stresses in the axisymmetric state at which the first non-axisymmetric bifurcation occurs ($m = 4$, $\Delta w_{\text{pole}} / \Delta w_{\text{R}} = 22.8$) are plotted in figure 9a and the

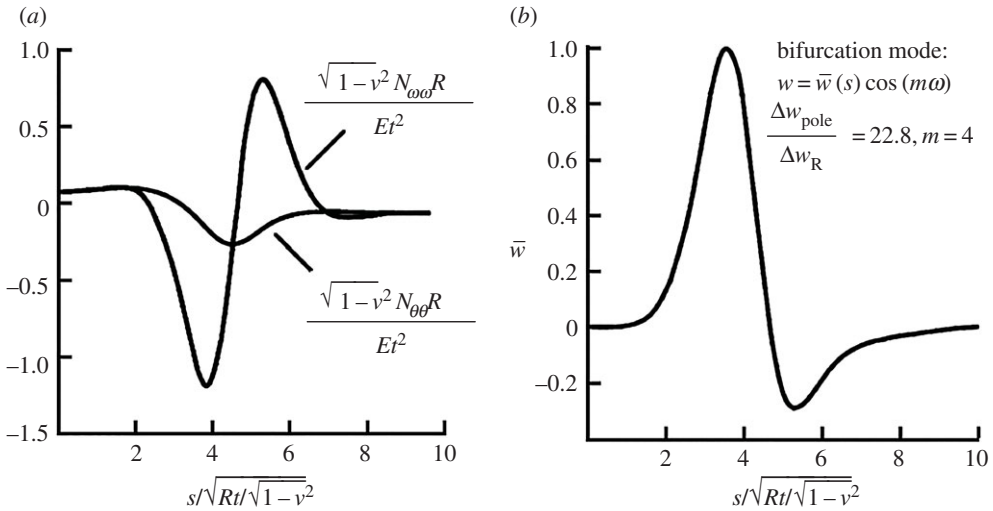


Figure 9. (a) Membrane stresses associated with the axisymmetric solution at $\Delta w_{\text{pole}}/\Delta w_{\text{R}} = 22.8$ corresponding to the lowest non-axisymmetric bifurcation ($m = 4$) for a spherical shell with $R/t = 300$ and $\nu = 0.3$. (b) The meridional shape of the associated bifurcation mode.

Table 2. First eigenvalue for non-axisymmetric bifurcation for wavenumber m .

m	4	5	6	7	8	9
$\Delta w_{\text{pole}}/\Delta w_{\text{R}}$	22.8	24.2	26.6	29.2	31.9	34.6
p/p_{C}	0.0964	0.0934	0.0888	0.0846	0.0808	0.0775

meridional shape of this non-axisymmetric mode is plotted in figure 9b. The scaled meridional distance from the pole \tilde{s} defined in (2.2) is used to emphasize the localization of the two distributions at the poles. The maximum compressive value of $N_{\omega\omega}$ in figure 9a is roughly twice the resultant membrane stress associated with p_{C} , i.e. $\sigma_{\text{C}}t = Et^2/(\sqrt{3(1-\nu^2)}R)$. It is primarily this compressive stress that drives the non-axisymmetric buckling, similar to the situation noted for cylindrical shells under axial compression with axisymmetric imperfections [22] and for spherical shells in the limiting buckled state with the top half buckling into the lower half [23]. Note that membrane stresses outside the dimple are very closely those of the uniform state, $N_{\omega\omega} = N_{\theta\theta} = pR/2$, and, therefore, very small compared with the maximum compressive stress within the dimple since $p/p_{\text{C}} \cong 0.1$ at $\Delta w_{\text{pole}}/\Delta w_{\text{R}} = 22.8$. The stress outside the axisymmetric dimple has almost no influence on non-axisymmetric buckling.

The results presented in table 2 and in figure 9b were computed using 35 uniformly spaced spline points on the interval $0 \leq \tilde{s} \leq \tilde{s}_{\text{edge}}$ with $\tilde{s}_{\text{edge}} = 12$. Computations were repeated with fewer spline points, with $\tilde{s}_{\text{edge}} = 10$ and 15, and with $R/t = 100$ and 200. Based on the sensitivities to these other choices, we judge the results in table 2 to be accurate to within several per cent for all shells with $R/t > 200$. The results for the pole deflection at bifurcation for $R/t = 100$ are approximately 10% smaller than those in table 2 and, for this case, a non-axisymmetric bifurcation with $m = 3$ was found at $\Delta w_{\text{pole}}/\Delta w_{\text{R}} = 19.0$. It should be noted, however, that condition (2.10) for shallowness and accuracy of the moderate rotation theory is marginally exceeded at bifurcation for these results when $R/t = 100$. It is also noted that the calculations were carried out assuming symmetry with respect to the equator for both the axisymmetric deformation and the non-axisymmetric mode. As already discussed, the localized nature of the buckling when the dimples are shallow essentially decouples behaviour at one pole from the other and thus the results in table 2 apply either to a single dimple at one pole or to symmetric dimples at the two poles.

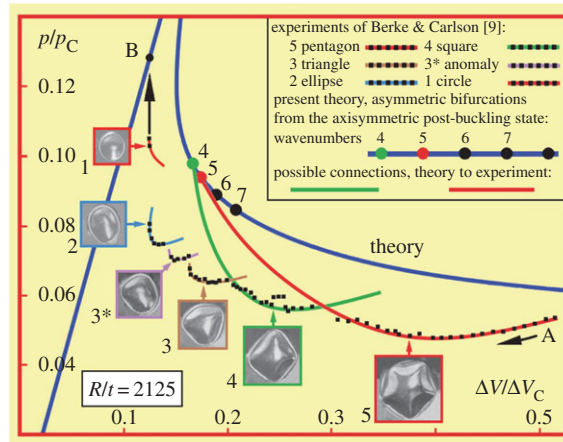


Figure 10. The results of Berke & Carlson [9] showing the changes in dimple shape and size during an unloading sequence, on a plot of pressure versus change of volume, both scaled relative to their critical values. In other tests with high-speed photography, these authors report that the dynamic buckling under dead load was first axisymmetric, but then fleetingly transformed through polygonal shapes, seeming to follow the reverse of the above static unloading test.

The non-axisymmetric modes reported by Quilliet [15] corresponded to a single dimple centred at the upper pole. As noted earlier, these modes cannot be quantitatively compared with those determined here because they were based on a strain energy density function for the shell that is different from that employed here. The mode appearing at the smallest value of ΔV was reported to have $m=6$ at a pole deflection somewhat larger than the minimum in the present case although still small enough to be nearly shallow. The mode with the smallest number of circumferential waves has $m=5$ as opposed to $m=4$ in the present case. Even if quantitative agreement is lacking, the qualitative similarity between the two sets of results obtained by very different numerical methods is striking.

The technique of manufacturing thin metal shells by electro-deposition onto a wax mandrel, initiated by Thompson [24] at Cambridge, UK, was dramatically developed at Stanford University, CA, under N. J. Hoff. The paper by Carlson *et al.* [25] describes how 32 complete spheres with radius-to-thickness ratios of around 2000 were produced by this electroforming. For specimens of good quality in optimal testing conditions, buckling pressures up to 86% of the classical value were obtained. The effect of the loading process was examined by pressurizing the shells in dead (pressure control) and rigid (volume control) conditions. That no difference in buckling pressure was observed effectively disproved the ‘energy criterion’ of Tsien [2].

Next, Berke & Carlson [9] reported further tests on high-precision electroplated nickel specimens with radius $R=4.25$ inches (10.8 cm) and thickness $t=0.002$ inches (0.005 cm), giving $R/t=2125$. Firstly, some volume-controlled tests were made with the wax mandrel still inside, though separated from the shell by a small gap. Here the mandrel has no effect on the initiation of the first dimple or upon its growth until the bottom of the dimple contacts the mandrel. At this contact strong oscillations induced transitions between several mode shapes, with often a large number of small dimples developing rapidly at other sites. High-speed motion pictures of the first inwards jump (from about $0.85 p_C$) suggested that for complete shells of large R/t buckling begins with an axisymmetric inwards dimple of small central angle.

With their very thin shells, and rigid loading, the authors [9] were able to perform post-buckling tests without the mandrel which nevertheless remained in the elastic range, offering repeatable results. Figure 10 shows a typical pressure–volume result for the *unloading* of a manually induced dimple in a single shell. This starts at point A, at a value of $\Delta V/\Delta V_C$ just over 0.5 with a five-sided ‘pentagonal’ dimple as shown in the inset photograph (5). The black squares represent the sequential results for the pentagonal dimples, from right to left, through which a red line has been fitted.

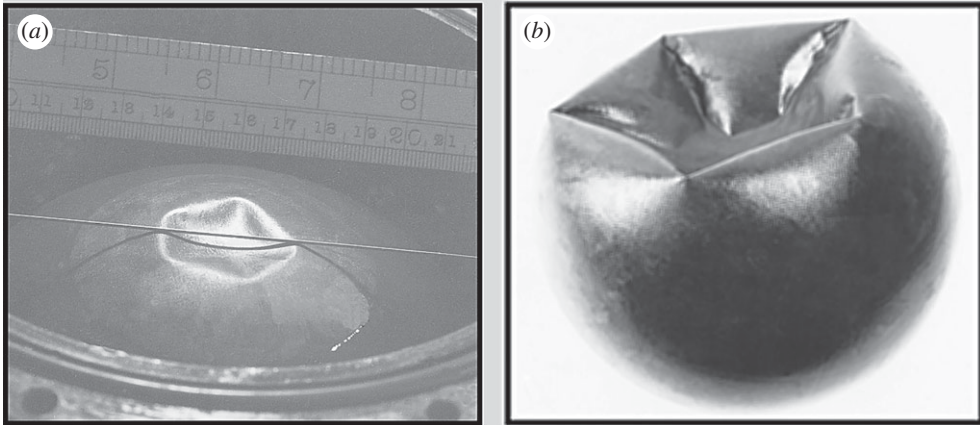


Figure 11. Final post-buckling configurations of two tests by Thompson [26] under rigid volume control (a) and prescribed pressure loading (b). Significant material yielding occurred during the dynamic jumps. Sizes nominally $R = 76$ mm, $t = 0.1$ mm ($R/t = 760$).

The pentagonal solution is lost when the shell jumps dynamically, at constant volume, from near the last, left-hand point of the red pentagon curve to the first, right-hand point of the green ‘square’ dimple path. We shall discuss the reason for this and the other jumps later. Under further slow controlled decrease of $\Delta V/\Delta V_C$ this pattern of events is repeated with jumps from square to ‘triangle’, triangle to an ill-defined ‘anomalous’ form, then to an ‘ellipse’, followed by a ‘circle’ and finally back to the trivial unbuckled solution at point B.

We must next think about the theoretical results of the present paper, which are of course for a perfect shell. The axisymmetric post-buckling path shown in deep blue in figure 10 has been computed using the results of §2 assuming that a single dimple forms. On this path are the four bifurcation points into non-symmetric modes with the wavenumbers $m = 4, 5, 6$ and 7 . Although not located in the current work, equilibrium paths with these numbers will emanate from the bifurcations, and it is tempting to see if paths from the four- and five-lobed dimples of the experimental observations could possibly link up with the predicted bifurcation points. The sketched connections do indeed look distinctly plausible.

The reasons for the experimental jumps seem to vary. The loss of stability under decreasing volume of the displayed experimental modes (1), (2), (3*) and (3) do seem to be at a fold (limit point) of vertical tangency, which is the most generic trigger for a dynamic jump. But the jumps from arcs (4) and (5), which we have already hypothesized might be connected to the theoretical bifurcations, do not seem to be from a well-defined vertical tangency.

Jumps from paths (4) and (5) need further consideration. On the one hand, there might be some underlying bifurcations of the paths. Alternatively, at these large deflections, there might be a high degree of sensitivity to dynamic disturbances. Berke and Carlson do indeed note that ‘the transition from one mode to another was very easily activated in the neighbourhood of the crossing points of two branches. Here a jump from one configuration to an adjacent one could be caused by a minor disturbance, even though the controlled volume was not changed.’ So some Maxwell considerations might be relevant in this arena.

Finally, it is historically interesting to note that large pentagonal post-buckled forms (with plastic yielding occurring during the jump) were observed in the experiments on electroplated copper shells by Thompson [26] in 1961 as illustrated in figure 11.

5. Conclusion

This paper has focused on the nonlinear buckling behaviour of the perfect spherical shell. In addition to an axisymmetric bifurcation mode, it is well known that thin, perfect spherical shells have many non-axisymmetric bifurcation modes associated with the critical buckling

pressure, p_C . If an imperfection or disturbance triggers a combination of both types of mode then asymmetric buckling is expected to occur, a possibility Koiter [4] addressed via his initial post-buckling approach. It is not understood why axisymmetric dimple buckles are so commonly observed in experiments given the existence of all the competing non-axisymmetric modes. However, the non-axisymmetric bifurcation analysis carried out here and earlier by Quilliet [15] for a different shell formulation has established that, once initiated, an axisymmetric dimple buckling resists deviations from axial symmetry until the buckle becomes quite deep, i.e. a dimple depth about twenty times the shell thickness. This goes some way to explaining why the axisymmetric dimple buckle is so prevalent, and why axisymmetric buckling behaviour reflects many of the interesting nonlinear aspects of spherical shell buckling. In this respect, spherical shells are more tractable from an analytical standpoint than cylindrical shells under axial compression because the axisymmetric behaviour of the latter does not reveal fundamental nonlinear aspects.

The contributions of the present paper build on the recent work [5,7,8] with particular emphasis on thin, perfect spherical shells in the range of buckling deflections relevant to structural behaviour. Using a shell formulation based on exact measures of bending and stretching, Hutchinson [5] has obtained accurate solutions of the axisymmetric post-buckling path of the complete spherical shell and has used them to establish the range of R/t such that moderate rotation theory is accurate. The path exhibits no minimum pressure prior to contact of the poles, so under dead loading there is no 'lower buckling load' as introduced by von Kármán & Tsien [1] or 'energy criterion load' introduced by Tsien [2], this latter now being called the Maxwell load as we have described earlier. The path was, moreover, shown to be stable against non-axisymmetric modes for small to moderate deflection magnitudes.

In this paper, we have exploited the shallow shell limit of moderate rotation theory which gives universal results with explicit R/t dependence within well-defined (and realistic) accuracy limits, and we have shown that the asymptotic shallow shell dimple analysis of Evkin *et al.* [12] provides an excellent approximation to this behaviour when the pole deflections become sufficiently large. We have checked the stability of the axisymmetric path against non-axisymmetric modes for higher deflections than before, and uncovered bifurcations into modes with wavenumbers progressing systematically from 4 to 9. These are shown to tie in well with experimental observations of the square and pentagonal dimples displayed in figure 10.

Returning to the universal axisymmetric solution, a dependency on R/t re-emerges when we plot (in figure 5) the pressure parameter, p/p_C , against the change of volume parameter, $\Delta V/\Delta V_C$. For rigid volume control this plot gives values of a minimum buckling volume change, ΔV_L , and a Maxwell volume change, ΔV_M , both functions of R/t as displayed in figure 6. To our knowledge, this paper for the first time presents accurate results for the Maxwell condition of equal energies in the unbuckled and buckled states over the entire practical range of R/t for rigid volume control. A neat extension covers the case of semi-rigid loading.

More important than the Maxwell points are the energy barriers [21] against finite static or dynamic disturbances plotted against the controlled $\Delta V/\Delta V_C$ in figure 7 for $R/t=100$. We compare the energy barriers for dead pressure and rigid volume control in figure 12 for the same R/t . The difference between these 'shock sensitivity' barriers is an indication of how much safer against disturbances is rigid volume control than dead pressure loading. For rigid volume control there exists no possibility of creating a buckle at pressures lower than that of point N, above L in figure 12*b*, and the curve for this case terminates at that pressure. The rather surprising fact that there is so little difference between the barriers of the perfect shell for the two extreme loadings is consistent with the fact that experiments on thin shells that have explored this issue have found very little dependency on loading compliance [25,27].

Initial imperfections must of course be considered if we are to improve on our current understanding of the scattered experimental results summarized recently by Wunderlich & Albertin [28]. An important step in that direction is made by Lee *et al.* [6], who have measured buckling pressures of elastomeric spherical shells of $R/t=108$ with carefully manufactured dimple imperfections with amplitudes up to 2.5 times the shell thickness. For imperfection

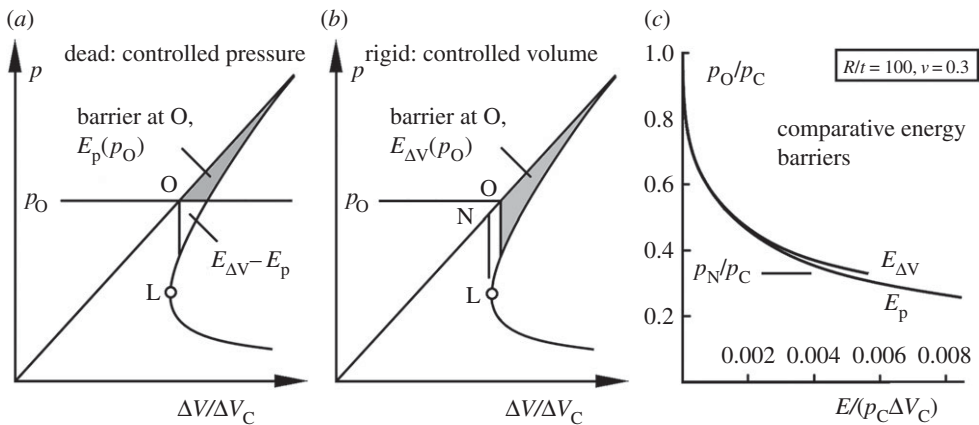


Figure 12. Sketches of the system energy barriers for (a) dead pressure, E_p , and (b) rigid volume control, $E_{\Delta V}$. With p_0 here as the pressure acting on the un buckled shell, E is the difference in the unstable buckled state from that in the un buckled state between the elastic energy in the shell plus the potential energy of the loading. The calculated energy barriers in (c) are for $R/t = 100$ and $\nu = 0.3$.

amplitudes greater than about one shell thickness, the measured buckling pressures are all about 20% of p_C . These values are less than half the lower limits of the existing datasets for the sphere (or the cylinder) at this R/t and similarly well below lower or Maxwell loads based on the perfect spherical shell discussed above. That such low values are not present in the existing datasets is almost certainly due to the fact that the shells with R/t as low as 100 do not have imperfections as large as those deliberately manufactured into the shells tested by Lee *et al.* [6].

Non-axisymmetric bifurcation from the axisymmetric buckled state revealed in this paper is qualitatively consistent with the multi-lobed dimples observed by Berke & Carlson [9] deep in the post-buckled range. It is obvious from the discussion in §4 that the bifurcation analysis is only a small beginning in the process of understanding the multiplicity of post-buckling solutions and the intriguing shapes they produce.

Authors' contributions. Both authors planned the study and participated in writing the paper. J.W.H. carried out the computations and J.M.T.T. prepared the figures.

Competing interests. We declare we have no competing interests.

Funding. We received no funding for this study.

Acknowledgement. The authors are indebted to C.R. Calladine for stimulating discussions which resulted in the inclusion of results for the strains in the shell in figure 4.

References

1. von Kármán T, Tsien HS. 1939 The buckling of spherical shells by external pressure. *J. Aeronaut. Sci.* **7**, 43–50. (doi:10.2514/8.1019)
2. Tsien HS. 1942 Theory for the buckling of thin shells. *J. Aeronaut. Sci.* **9**, 373–384. (doi:10.2514/8.10911)
3. Koiter WT. 1945 On the stability of elastic equilibrium. Dissertation, Polytechnic Institute of Delft, Delft, The Netherlands. (An English translation is available as *NASA Tech. Trans. F 10 833*, 1967.)
4. Koiter WT. 1969 The nonlinear buckling problem of a complete spherical shell under uniform external pressure, parts I, II, III and IV. *Proc. Kon. Ned. Akad. Wet. B* **72**, 40–123.
5. Hutchinson JW. 2016 Buckling of spherical shells revisited. *Proc. R. Soc. A* **472**, 20160577. (doi:10.1098/rspa2016.0577).
6. Lee A, Marthelot J, Jimenez FL, Hutchinson JW, Reis PM. 2016 The geometric role of precisely engineered imperfections on the critical buckling load of spherical elastic shells. *J. Appl. Mech.* **83**, 111005. (doi:10.1115/1.4034431)

7. Knoche S, Kierfeld J. 2011 Buckling of spherical capsules. *Phys. Rev. E* **84**, 046608-1-13. (doi:10.1103/PhysRevE.84.046608)
8. Knoche S, Kierfeld J. 2014 Osmotic buckling of spherical capsules. *Soft Matter*, **10**, 8358–8369. (doi:10.1039/C4SM01205D)
9. Berke L, Carlson RL. 1968 Experimental studies of the post buckling behaviour of complete spherical shells. *Exp. Mech.* **8**, 548–553. (doi:10.1007/BF02327517)
10. Sanders JL. 1963 Nonlinear shell theories for thin shells. *Q. Appl. Math.* **21**, 21–36. (doi:10.1090/qam/147023)
11. Koiter WT. 1966 On the nonlinear theory of thin elastic shells. *Proc. Kon. Ned. Akad. Wet.* **B69**, 1–54.
12. Evkin A, Kolesnikov M, Prikazchikov DA. 2016 Buckling of a spherical shell under external pressure and inward concentrated load: asymptotic solution. *Math. Mech. Solids* **1**, 1–13. (doi:10.1177/1081286516635872)
13. Holst JMFG, Calladine CR. 1994 Inversion problems in elastic shells. *Eur. J. Mech. A Solids* **13**, 3–18.
14. Thompson JMT. 1964 The rotationally-symmetric branching behaviour of a complete spherical shell. *Proc. R. Neth. Acad. Sci.* **67**, 295–311.
15. Quilliet C. 2012 Numerical deflation of beach balls with various Poisson's ratios: from sphere to bowl's shape. *Eur. Phys. J. E* **35**, 48-1-9. (doi:10.1140/epje/i2012-12048-3)
16. Tsien HS. 1947 Lower buckling load in the non-linear buckling theory for thin shells. *Q. Appl. Math.* **5**, 236–237. (doi:10.1090/qam/99994)
17. Hunt GW, Peletier MA, Champneys AR, Woods PD, Ahmer Wadee M, Budd CJ, Lord GJ. 2000 Cellular buckling in long structures. *Nonlinear Dyn.* **21**, 3–29. (doi:10.1023/A:1008398006403)
18. Thompson JMT. 2015 Advances in shell buckling: theory and experiment. *Int. J. Bifurcation Chaos* **25**, 1530001. (doi:10.1142/S0218127415300013)
19. Thompson JMT, van der Heijden GHM. 2014 Quantified shock-sensitivity above the Maxwell load. *Int. J. Bifurcation Chaos* **24**, 1430009. (doi:10.1142/S0218127414300092)
20. Horák J, Lord GJ, Peletier MA. 2006 Cylinder buckling: the mountain pass as an organizing centre. *SIAM J. Appl. Math.* **66**, 1793–1824. (doi:10.1137/050635778)
21. Thompson JMT, Sieber J. 2016 Shock-sensitivity in shell-like structures: with simulations of spherical shell buckling. *Int. J. Bifurcation Chaos* **26**, 1630003. (doi:10.1142/S0218127416300032)
22. Koiter WT. 1963 The effect of axisymmetric imperfections on the buckling of cylindrical shells under axial compression. *Proc. Kon. Ned. Akad. Wet.* **66**, 265–279.
23. Knoche S, Kierfeld J. 2014 The secondary buckling transition: wrinkling of buckled spherical shells. *Eur. Phys. J. E* **37**, p62-1-21. (doi:10.1140/epje/i2014-14062-9)
24. Thompson JMT. 1960 Making of thin metal shells for model stress analysis. *J. Mech. Eng. Sci.* **2**, 105–108. (doi:10.1243/JMES_JOUR_1960_002_019_02)
25. Carlson RL, Sendelbeck RL, Hoff NJ. 1967 Experimental studies of the buckling of complete spherical shells. *Exp. Mech.* **7**, 281–288. (doi:10.1007/BF02327133)
26. Thompson JMT. 1961 The elastic instability of spherical shells. PhD dissertation, Clare College, Cambridge University, Cambridge, UK.
27. Babcock CD. 1983 Shell stability. *J. Appl. Mech.* **50**, 935–940. (doi:10.1115/1.3167206)
28. Wunderlich W, Albertin U. 2002 Buckling behavior of imperfect spherical shells. *Int. J. Nonlin. Mech.* **37**, 589–604. (doi:10.1016/S0020-7462(01)00086-5)